Exponential growth of an unstable l=1 diocotron mode for a hollow electron column in a warmfluid model

S. N. Rasband, Ross L. Spencer, and Richard R. Vanfleet

Citation: Physics of Fluids B: Plasma Physics (1989-1993) **5**, 669 (1993); doi: 10.1063/1.860512
View online: http://dx.doi.org/10.1063/1.860512
View Table of Contents: http://scitation.aip.org/content/aip/journal/pofb/5/3?ver=pdfcov
Published by the AIP Publishing

Exponential growth of an unstable $l=1$ diocotron mode for a hollow electron column in a warm-fluid model

S. N. Rasband, Ross L. Spencer, and Richard R. Vanfleet
Department of Physics and Astronomy, Brigham Young University, Provo, Utah 84602

(Received 17 June 1992; accepted 2 December 1992)

Numerical investigations of a warm-fluid model with an isothermal equation of state for the perpendicular dynamics of an axisymmetric, magnetically confined pure electron plasma predict an exponentially unstable, $l=1$, diocotron mode for hollow density profiles. The unstable mode can be identified with a stable, nonsmooth mode that exists in cold drift models but which is destabilized by finite temperature effects. The unstable mode has many properties similar to the experimental results reported by Driscoll [Phys. Rev. Lett. **64**, 645 (1990)].

I. INTRODUCTION

In a recent letter Driscoll[1] discussed experimental observations of an $l=1$ exponentially unstable diocotron mode in a hollow electron column. In a conventional two-dimensional (2-D) drift model (no inertia and zero temperature), linear theory predicts that there are no $l=1$ exponentially unstable modes. In a companion article Smith and Rosenbluth[2] described analytic and numerical investigations of the same system with the same 2-D drift model. They find algebraic growth of $l=1$ perturbations $\propto \sqrt{t}$, but no exponentially growing instabilities like those seen in the experiment.[1] In a subsequent letter Smith[3] explored the effects of finite gyroradius and, in a phenomenological way, the effects of finite axial length on exponential growth. The purpose of this paper is to present results from a numerical investigation of linear stability in a 2-D fluid model with finite temperature. We find that an $l=1$ exponentially unstable mode exists with frequency, growth rate, and mode structure comparable with experimental values. The dependence of the growth rate on temperature and on the hollowness of the density profile is explored.

The simplified physical model we adopt for the plasma is that of a collection of electrons confined axially by electrostatic forces in a cylindrical, conducting container and confined radially by a strong axial magnetic field. To describe the electrons, with charge $-e$, we adopt a collisionless fluid model. The resulting equations represent one of the simplest models for a plasma and may be found in most standard text books.[4] We adopt cylindrical coordinates (r, θ, z) and further assume that the electron column is long so that we can ignore the axial coordinate z. The magnetic field is assumed to consist simply of the applied field aligned along z, since for nonrelativistic motion of the electrons the magnetic fields generated by their motions are negligible.[5] We further assume a scalar pressure in the perpendicular directions and focus on the fields $n(r, \theta, t)$, $\mathbf{V}(r, \theta, t)$, and $\Phi(r, \theta, t)$ representing the electron number density, velocity, and electrostatic potential, respectively. We assume that there is no axial flow, i.e., $V_z \equiv 0$. We explicitly *do not* assume the plasma to be cold and take the perpendicular pressure to be $kTn(r, \theta, t)$ with T constant and we *do not* discard the inertial terms as being small. The assumption of constant temperature in the scalar pressure is a very strong simplifying assumption which is known to give poor results in at least some cases. However, it does introduce an important feature that will persist in more correct models, but which is missing from Smith's calculation, namely, the raising of the spatial order of the differential equations from second to fourth. (Some models may give even higher order.) This effect has a strong influence on the dynamics of our model (see the oscillations in Figs. 3 and 4) and is presumably also important in better models which also raise the order. Before proceeding to the study of these better, and more complicated models, we feel it is important to understand the predictions of the simple constant-temperature model.

II. EQUILIBRIUM AND STABILITY

In the usual way we consider a perturbation away from an equilibrium configuration and examine the linear stability of the perturbation. For an equilibrium flow of the electron fluid that is axisymmetric and only azimuthal, the continuity equation is identically satisfied for any given equilibrium density profile $n_0(r)$. Momentum balance for the fluid is contained in the equilibrium equation

$$m_e \mathbf{V}_0 \cdot \nabla \mathbf{V}_0 + \frac{kT}{n_0} \nabla n_0 = e \nabla \Phi_0 - \frac{e}{c} \mathbf{V}_0 \times \mathbf{B}, \tag{1}$$

wherein centrifugal forces, pressure forces, and electrostatic repulsion are all balanced by the magnetic force. The electrostatic potential follows from the chosen number density $n_0(r)$ through Poisson's equation. Once $n_0(r)$ is specified, Eq. (1) is used simply to obtain the equilibrium flow $V_\theta(r)$. In a cold-plasma approximation with zero electron mass, the left-hand side of (1) is set equal to zero resulting in simple $\mathbf{E} \times \mathbf{B}$ drift motion for the equilibrium electron column. The inclusion of the centrifugal and pres-

 0899-8221/93/030669-05$06.00

sure forces in (1) leads to a more general expression for the equilibrium fluid velocity. With $\Omega = eB/m_e c$ and $r\omega_0(r) = V_\theta(r)$,

$$\omega_0(r) = \frac{\Omega}{2}\left(1 - \sqrt{1 - \frac{4}{\Omega}\left[\omega_E(r) + \omega_D(r)\right]}\right), \tag{2}$$

where $\omega_E(r) = (c/rB)d\Phi_0/dr$ and $\omega_D(r) = -(ckT/eBrn_0)dn_0/dr$ are the familiar $\mathbf{E}\times\mathbf{B}$ and diamagnetic drifts, respectively. It is the presence of the diamagnetic drift in the rotation profile and the retention of the inertial terms in the perturbation equations that lead to the temperature effects reported here.

In the fluid model there are four coupled equations for the four perturbation fields: $\delta n(r,\theta,t)$, $\delta V_\theta(r,\theta,t)$, $\delta V_r(r,\theta,t)$, and $\delta\Phi(r,\theta,t)$. Since the azimuthal modes separate, we Fourier decompose these fields by assuming an angular dependence of the form $\exp(il\theta)$. The stability of each l mode can then be examined separately and we focus on the linearized dynamics for the field perturbations $\delta n_l(r,t)$, $\delta V_{l\theta}(r,t)$, $\delta V_{lr}(r,t)$, $\delta\Phi_l(r,t)$ for each l mode:

$$\frac{\partial \delta n_l}{\partial t} + \frac{1}{r}\frac{\partial}{\partial r}(r n_0 \delta V_{lr}) + \frac{il}{r} n_0 \delta V_{l\theta} + il\omega_0 \delta n_l = 0, \tag{3}$$

$$\frac{\partial}{\partial t}(n_0 \delta V_{lr}) + (\Omega - 2\omega_0) n_0 \delta V_{l\theta} + il\omega_0 n_0 \delta V_{lr} - \frac{kT}{m_e}\frac{n_0'}{n_0}\delta n_l + \frac{kT}{m_e}\frac{\partial \delta n_l}{\partial r} = \frac{en_0}{m_e}\frac{\partial \delta\Phi_l}{\partial r}, \tag{4}$$

$$\frac{\partial}{\partial t}(n_0 \delta V_{l\theta}) + \left(\frac{1}{r}(r^2\omega_0)' - \Omega\right) n_0 \delta V_{lr} + il\omega_0 n_0 \delta V_{l\theta} + \frac{il}{r}\frac{kT}{m_e}\delta n_l = \frac{en_0}{m_e}\frac{il}{r}\delta\Phi_l, \tag{5}$$

$$\frac{1}{r}\frac{\partial}{\partial r}\left(r\frac{\partial}{\partial r}\delta\Phi_l\right) - \frac{l^2}{r^2}\delta\Phi_l = 4\pi e \delta n_l. \tag{6}$$

Derivatives with respect to r of equilibrium quantities are denoted with primes.

Boundary conditions follow from imposing regularity at $r=0$ and requiring the perturbations to vanish at $r=r_{\text{wall}}$. Equations (3)–(6) for the perturbed fields recognizably stem from mass balance, momentum balance, and Poisson's equation.

Because the initial results were surprising, i.e., exponentially growing solutions in a plasma model that differs from previous studies only by $T\neq 0$ and the inclusion of inertial effects, and because the differential equations are stiff and singular as $T\to 0$, we have labored to obtain numerical solutions to the linearized perturbation equations in three substantially different ways.

However, before discussing our various numerical approaches, we note that Eqs. (3)–(6) lead to a fourth-order differential equation for either the perturbed density δn or the perturbed potential $\delta\Phi$. This is in contrast to the second-order equations obtained in cold drift theory, Eq. (1) in Ref. 2, or the finite Larmor radius (FLR) modified version of this equation given by Smith, Eq. (10) of Ref. 3. This fourth-order equation has as a singular limit the familiar second-order equation and results only when inertial terms are kept as well as nonzero temperature. To simply augment the electric drift ω_E by the diamagnetic drift ω_D in the second-order equation would be inconsistent and lead to unreliable results. We have also briefly studied the equations that result from including off-diagonal contributions from FLR effects in the electron pressure tensor. The resulting mode equation for say the perturbed density is fifth order. The increased complexity and degree of the mode equation is very likely a feature of any physical model that is an improvement over the simple cold drift theory. We now describe briefly the three methods used for obtaining numerical solutions to Eqs. (3)–(6) with the appropriate boundary conditions.

III. NUMERICAL SOLUTIONS

(1) We first developed an eigenvalue code to solve Eqs. (3)–(6). The radial interval $[0, r_{\text{wall}}]$ was divided into N finite elements and then the perturbed fields for each l mode were expanded in terms of a set of cubic B splines that appropriately satisfy the boundary conditions at $r=0$ and $r=r_{\text{wall}}$. We then followed a standard Galerkin procedure to reduce the partial differential equations to a set of four, coupled, ordinary differential equations. In this manner we obtained a linear system $\dot{\mathbf{x}}_l = \mathbf{D}_l \mathbf{x}_l$, where the vector $\mathbf{x}_l$ is a composite vector made up of the spline expansion coefficients for the perturbed fields. The matrix operator $\mathbf{D}_l$ has elements that consist of integrals of spline functions with equilibrium profiles $n_0(r), \omega_0(r)$, and their derivatives. Thus, once the equilibrium density profile has been specified, all elements of $\mathbf{D}_l$ can be computed. The stability of the specified profile was then determined by computing the eigenvalues of the matrix $\mathbf{D}_l$. The matrix $\mathbf{D}_l$ is generally complex without symmetry. It is comprised of submatrix blocks that are typically symmetric, banded, and either real or imaginary. We computed the complex eigenvalues and eigenvectors of this matrix using a double precision version of a routine for finding eigenvalues and eigenvectors of complex matrices from the SLATEC library.[6] We determined the physically meaningful eigenvalues by examining the radial dependence of the eigenfunctions.

(2) For the next two codes we assumed a time dependence of the form $\exp(-i\omega t)$, which then leads to the replacement of $\partial/\partial t$ by $-i\omega$ in Eqs. (3)–(6). The object then became the following: find the perturbed fields and ω such that Eqs. (3)–(6) along with the boundary conditions are satisfied. The radial interval was divided into finite elements and the perturbed fields $\delta\Phi_l$ and δn_l were expanded in spline functions as described under method (1). Through the usual Galerkin procedure of multiplying Eq. (6) by an expansion function $\psi_i(r)$ and then integrating over the interval $(0, r_{\text{wall}})$, we obtained a relationship between the spline expansion coefficients for $\delta\Phi_l$ in terms of those for δn_l. Equations (4) and (5) were solved for δV_{lr} and $\delta V_{l\theta}$ in terms of $\delta\Phi_l$ and δn_l and their derivatives.

Equation (3) was subjected to the same Galerkin procedure and the term involving $r^{-1}d(rn_0\delta V_{lr})/dr$ was integrated by parts. The homogeneous boundary conditions on the spline functions eliminate the integrated term. Upon substitution of the equations obtained for δV_{lr} and $\delta V_{l\theta}$, we were left with a so-called weak formulation of the eigenvalue problem involving the spline expansion coefficients of δn_l that was then solved in a straightforward way.

(3) Our third method of solution was based on an inertial expansion of the drift velocities using the balance equations for mass and momentum:

$$\frac{\partial n}{\partial t}+\nabla\cdot(n\mathbf{V})=0, \tag{7}$$

$$m_e\left(\frac{\partial \mathbf{V}}{\partial t}+\mathbf{V}\cdot\nabla\mathbf{V}\right)=-e\mathbf{E}-\frac{e}{c}\mathbf{V}\times\mathbf{B}-\frac{kT}{n}\nabla n. \tag{8}$$

Assuming the inertial terms on the left in (8) are small, for $\mathbf{V}=\mathbf{V}^0+\mathbf{V}^1$, we obtain

$$\mathbf{V}^0=c\left(\frac{-\nabla\Phi}{B}+\frac{kT}{eB}\frac{\nabla n}{n}\right)\times\hat{\mathbf{z}}, \tag{9}$$

$$\mathbf{V}^1=\frac{1}{\Omega}\left(\frac{\partial \mathbf{V}^0}{\partial t}+\mathbf{V}^0\cdot\nabla\mathbf{V}^0\right)\times\hat{\mathbf{z}}. \tag{10}$$

Substituting $\Phi=\Phi_0+\delta\Phi$ and $n=n_0+\delta n$ into Eqs. (7), (9), and (10) leads, after a somewhat lengthy calculation, to a second-order differential equation for δn involving $\delta\Phi$, $d\delta\Phi/dr$, the equilibrium density and rotation profiles, and derivatives of these profiles. This expression for $d^2\delta n/dr^2$ in a twice differentiated form of Poisson's equation, leads to a fourth-order differential equation in $\delta\Phi$ involving the eigenvalue ω. This eigenvalue problem is solved by "shooting" outward from $r=0$ and inward $r=r_{\rm wall}$ with matching conditions at some interior point.

The results of all three codes were compared and checked against each other. Also in the $T=0$ limit they were checked against analytic results for flat profiles[7] and the results from an earlier code for cold drift dynamics.[8] For $l=1$ modes in cold, hollow profiles the codes correctly identify the fundamental $l=1$ diocotron mode with $\omega=\omega_E(r_{\rm wall})\equiv\omega_1$ *and* a second stable mode with $\omega=\omega_{E\,\max}\equiv\omega_2$, where $\omega_{E\,\max}$ and $r_{\max}$ correspond to the values of $\omega_E(r)$ and r where $d\omega_E/dr=0$. In the cold drift model the first of these stable modes has an analytic solution for the perturbed potential proportional to $r[\omega_1-\omega_E(r)]$.[9] The second stable mode has a nonsmooth perturbed potential: it is proportional to $r[\omega_2-\omega_E(r)]$ for $0<r<r_{\max}$ and is identically zero for $r_{\max}<r<r_{\rm wall}$. This is the same mode that Smith and Rosenbluth find leading to algebraic instability.[2] Since the perturbed potential for this second mode vanishes over a finite interval including $r_{\rm wall}$, the mode makes no electric field at the wall and is hence invisible to sectored wall detectors used in experiments to detect image charges in the conducting wall. Such a mode has been referred to as self-shielding.[1]

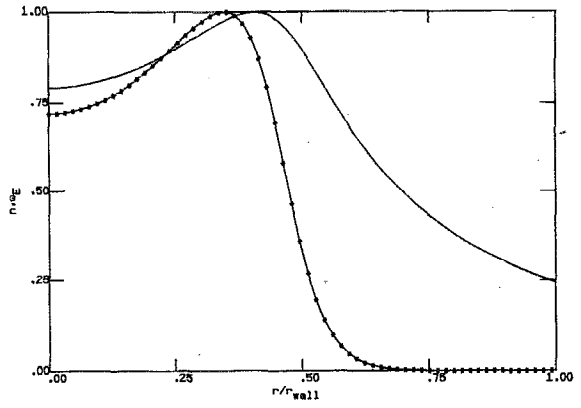

FIG. 1. The $n_0(r)$ and $\omega_E(r)$ profiles for the parameter values given in the text. The number density, with asterisks on the curve, is normalized to the peak value of 5.00×10^6 cm^{-3} and the frequency is normalized to its peak value of 1.097×10^6 sec^{-1}.

This self-shielding mode is precisely that mode which we calculate to be unstable with the inclusion of finite temperature. We consider the identification of this $l=1$ instability with that seen in experiment as likely based on the following discussion.

IV. DEPENDENCE OF GROWTH RATE ON TEMPERATURE AND HOLLOWNESS

For this study we used a density function of the form

$$n_0(r)=\hat{n}[1+\mu_1(r/r_p)^2]\exp[-(r/r_p)^{\mu_2}], \tag{11}$$

where $\hat{n}$ is the central density, μ_1 controls the hollowness of the profile, μ_2 controls the steepness of the cutoff, and r_p controls the position of the cutoff. Figure 1 displays $n_0(r)$ and $\omega_E(r)$ for the values $\hat{n}=3.6\times10^6$ cm^{-3}, $\mu_1=0.95$, $r_p/r_{\rm wall}=0.47$, $\mu_2=8$, $r_{\rm wall}=3.81$ cm. These values were chosen with the aim of giving a comparable profile to the graph given in Fig. 3 of Ref. 1. In situations with high temperatures ($\gtrsim28$ eV) where $d\ln n_0(r)/dr$ can become large and consequently ω_D become large enough so that the argument under the square root sign in Eq. (2) becomes negative, we have matched the profile of Eq. (11) to one of the form $A(1+Cx+Dx^2)\exp(-Bx)$, where the constants are chosen so as to match up through three derivatives. To within a few percent, mode frequencies and growth rates are insensitive to such details in the density profile. In other words, the complex mode frequencies are insensitive to the behavior of ω_D in the tail of the density profile.

Using $n_0(r)$ from Eq. (11) with $T=1.2$ eV and the values of the parameters as given, we find a mode frequency of $f_u=175$ kHz and a growth rate $\gamma_u=2.9\times10^3$ sec^{-1}. These values are to be compared with the experimental measurements reported in Ref. 1: $f_u=143.4$ kHz and $\gamma_u=23.3\times10^3$ sec^{-1}. The growth rate is lower than that observed experimentally by a factor ~8. However, it is difficult to assess the significance of this discrepancy because the growth rate is strongly temperature and profile

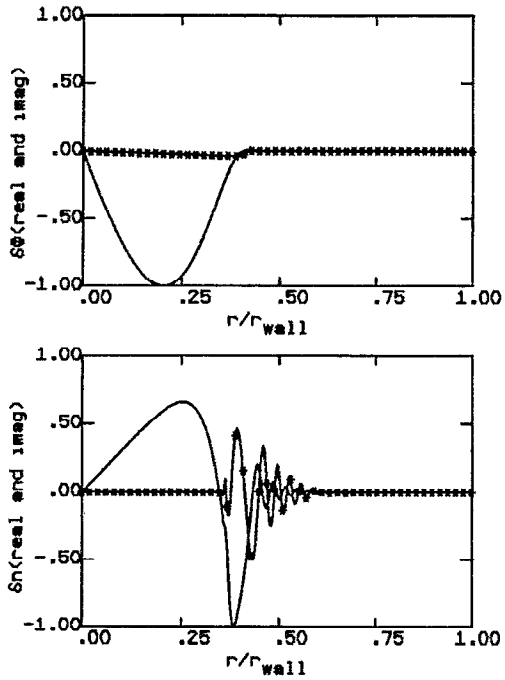

FIG. 2. Perturbed eigenfunctions for the potential and the density showing the real and imaginary parts. The imaginary parts are indicated with the asterisks. The functions are normalized to the maximum absolute value in the real part of the eigenfunction. The equilibrium profiles for these perturbed functions are given in Fig. 1.

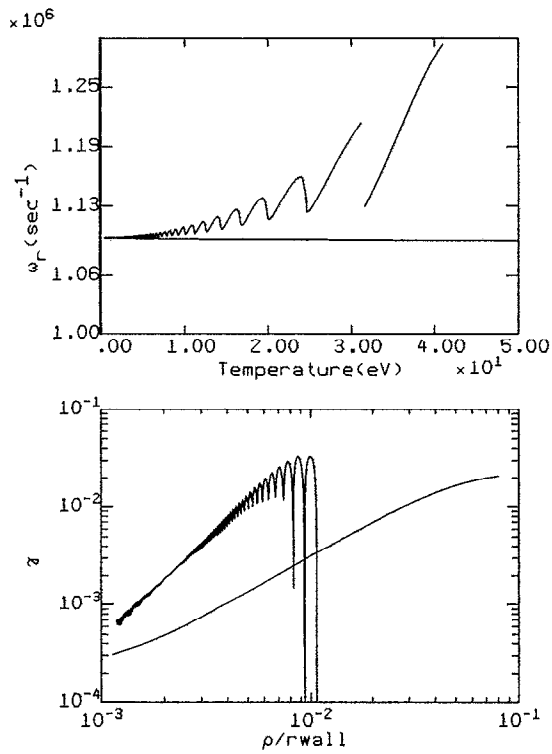

FIG. 3. A plot of the real part of the eigenvalue ω_r as a function of temperature and a plot of the imaginary part γ, scaled by (central plasma frequency)^2/(gyrofrequency) $=1.74\times10^6$ (sec^{-1}), as a function of the scaled gyroradius. The gaps in the trace of ω_r are over temperature intervals where the mode frequency has zero growth rate. The lower traces in these plots are the results from using the model in Eq. (10) of Ref. 3 and any differences in the values from those shown in Fig. 3 of that paper are fully accounted for by differences in the density profiles and the scaling. We use the density profile shown in Fig. 1.

dependent. For comparison cold drift codes for $l=2$, hollow profile instabilities give growth rates typically low by a factor ~2.[8]

The eigenfunctions for the unstable mode at $T=1.2$ eV and for the profile given in Fig. 1 are plotted in Fig. 2. The fact that this mode is self-shielding is evident from the vanishing of the perturbed potential over a finite interval, implying zero perturbed electric field at the wall. The imaginary part of the density perturbation begins at the r value where $\omega_{\text{real}}=\omega_0(r)$ and oscillates while going to zero at $r/r_{\text{wall}}\sim0.7$. The reason for the appearance of an imaginary part for δn at this point in the profile is that the zero-temperature, second-order, radial differential equation with continuous spectrum $\omega_E(r)$ has here been replaced by a fourth-order radial differential equation with a new continuous spectrum $\omega_0(r)=\omega_E(r)+\omega_D(r)$. It is the resonance of the mode near $\omega_{E\,\max}$ with the new continuum that gives rise to instability and the appearance of oscillations in Fig. 2. The number of visible oscillations between the "birth" and "death" of the imaginary part of the density eigenfunction depends on the value of the temperature, with the number of oscillations increasing as T decreases toward zero. The maximum absolute value in the plots of the eigenfunctions in Fig. 2 is set equal to 1.0.

Figure 3 shows a plot of the eigenvalue for the unstable $l=1$ diocotron mode as a function of the temperature. For purposes of comparison we have included in Fig. 3 the curves resulting from Eq. (10) of Ref. 3. These are the lower traces in the figure, without oscillations, and agree

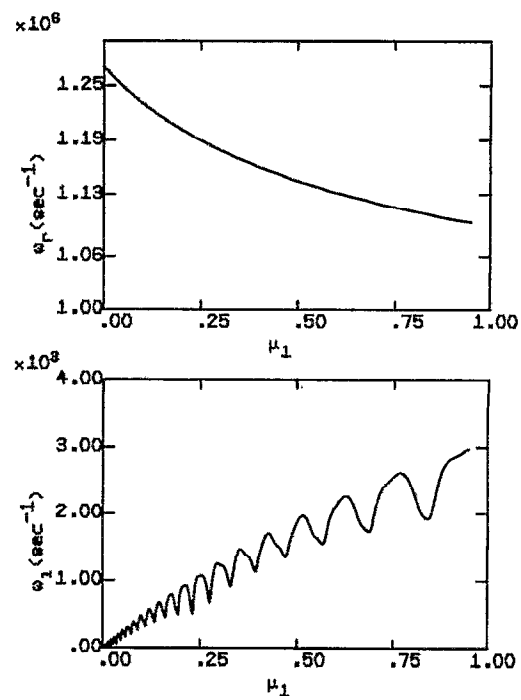

FIG. 4. A plot of the eigenvalue (real part ω_r and imaginary part ω_i) as a function of the hollowness of the profile as determined by the parameter μ_1 defined in Eq. (11). The parameter $\hat{n}$ is also adjusted to keep the total number of particles per unit length a constant. The remaining parameters of the profile are held constant and $T=1.2$ eV.

with the results of Ref. 3 when appropriately adjusted for scaling and profile differences. Figure 4 is a similar plot of the eigenvalue at $T=1.2$ eV as a function of the parameter μ_1 determining the hollowness of the profile. The real part of the eigenvalue ω is denoted as ω_r and the imaginary part, or growth rate, is denoted as ω_i. The last two of the codes previously described were used to check on the agreement between the positions of the peaks and valleys in these figures as well as the actual values and were found to be typically within 1% or better.

Given the uncertainties in the profile, the approximations inherent in a finite temperature fluid code that includes only perpendicular dynamics and constant temperature, and the usual experimental uncertainties in measured values, we find the evidence suggestive that a significant contribution to the growth of the $l=1$ unstable mode observed by Driscoll[1] results from the fluid diamagnetic drift and the inclusion of inertia. Furthermore, the mode is tentatively identified as the stable $l=1$ mode with frequency ω_2 and with nonsmooth potential perturbation that exists in the 2-D cold drift approximation for hollow profiles.[9] A subsequent theoretical investigation of the unstable $l=1$ diocotron mode should proceed from a more detailed model including not only finite temperature but also involving dynamics along the magnetic field lines so that the importance of finite length effects can be explored self-consistently.

ACKNOWLEDGMENT

The authors wish to acknowledge helpful discussions with our colleague Grant Hart on many aspects of this work.

[1]C. F. Driscoll, Phys. Rev. Lett. **64**, 645 (1990).
[2]R. A. Smith and M. N. Rosenbluth, Phys. Rev. Lett. **64**, 649 (1990).
[3]R. A. Smith, Phys. Fluids B **4**, 287 (1992).
[4]For example, R. C. Davidson, *Physics of Nonneutral Plasmas* (Addison-Wesley, New York, 1990), Sec. 2.3.
[5]See Ref. 4, Chap. 5.
[6]The SLATEC library is available through the U.S. Department of Energy, National Energy Software Center, 9700 Cass Ave., Argonne, IL 60439.
[7]R. J. Briggs, J. D. Daugherty, and R. H. Levy, Phys. Fluids **13**, 421 (1970).
[8]R. L. Spencer, Phys. Fluids B **2**, 2306 (1990).
[9]R. H. Levy, Phys. Fluids **11**, 920 (1968).